Journal of Nuclear Materials 377 (2008) 21–27

Contents lists available at ScienceDirect

Journal of Nuclear Materials

journal homepage: www.elsevier.com/locate/jnucmat

Present status of study on development of materials resistant to radiation and beam impact

M. Kawai [a,*], H. Kokawa [b], M. Michiuchi [b], H. Kurisihita [c], T. Goto [d], M. Futakawa [e], T. Yoshiie [f], A. Hasegawa [b], S. Watanabe [g], T. Yamamura [b], N. Hara [b], A. Kawasaki [b], K. Kikuchi [e]

[a] Institute of Materials Structure Science, High Energy Accelerator Research Organization, Oho, Tsukuba-shi, Ibaraki-ken 305-0801, Japan
[b] Graduate School of Engineering, Tohoku University, Aramaki-aza-Aoba, Aoba-ku, Sendai 980-8579, Japan
[c] International Research Center for Nuclear Material Science, Tohoku University, Narita-cho, Oarai, Ibaraki-ken 311-1313, Japan
[d] Graduate School of Energy Science, Kyoto University, Sakyo-ku, Kyoto 606-8501, Japan
[e] Quantum Beam Science Directorate, Japanese Atomic Energy Agency, Tokai-mura, Ibaraki-ken 319-1195, Japan
[f] Research Reactor Institute, Kyoto University, Kumatori-cho, Sennan-gun, Osaka-fu 590-0494, Japan
[g] Center for Advanced Research of Energy Conversion Materials, Hokkaido University, Kita-ku, Sapporo 060-8628, Japan

A B S T R A C T

Pulsed spallation neutron sources for the materials structure science are severely influenced by beam impact and radiation damage. We have developed the materials strong to these influence since 2004. In this paper, recent topics are described concerning the development of intergranular corrosion (IGC)-resistant austenitic stainless steel for target vessel and window, radiation-resistant ultra-fine grained tungsten materials (W–TiC) for a solid target, CrN film on a tungsten target by means of a molten-salt method, surface treatment of stainless steel for pitting damage in mercury target. Bubble behavior at the interface of mercury and window glass was also observed to clarify the phenomenon of the pitting damage.

1. Introduction

Materials which have strong resistance to both beam impact and radiation damage are required for the intense spallation neutron sources for the material science as well as the accelerator driven system for transmitting long lived nuclides in the used nuclear fuel to shorter one. The present work has been made for the purpose of developing such intelligent materials tough to both irradiation damage and mechanical stresses such as shock-wave due to beam impact as well as to corrosion [1]. The issues to be studied are stainless steel improvement and its compatibility with a coolant: intergranular corrosion crack in case of a solid target and the pitting damage by beam impact in case of a mercury target, improvement of radiation damage property of tungsten and cladding technique of tungsten against corrosion by water. This paper describes the present status of activities for spallation materials of both solid and liquid metal targets since the previous workshop, IWSMT-7.

Stainless steel is a major material of target vessel and beam window of the spallation neutron sources. In constructing a structure, welding is required. Intergranular corrosion (IGC) by a coolant water, resulting in weld decay [2,3], is frequently observed in the heat affected zone (HAZ) of austenitic stainless steel. IGC is initially caused by $Cr_{23}C_6$ precipitation in the grain boundary. Chromium carbide precipitation leads to sensitization by chromium depletion. Such sensitization cannot perfectly be prevented by previous conventional techniques, such as reducing the carbon content, a stabilization treatment, and a local solution heat treatment. Recent studies on the grain boundary structure have revealed that the sensitization depends strongly on the crystallographic nature and the atomic structure of the grain boundary, and that low-energy grain boundaries, such as CSL (coincidence site lattice) boundaries, have strong resistance to IGC [4,5]. The concept of 'grain boundary design and control' [6] has been developed through GBE (grain boundary engineering) [7] to inhibit sensitization by increasing the frequency of CSL boundaries. GBE was applied to austenitic stainless steels which will have superior resistance even usage for HAZ by welding [3,8,9]. The present GBE process is composed of solution-heating, cold-rolling as a pre-strain and annealing. In the present work, the effect of the pre-strain was investigated and an optimum condition was found out for 316-type stainless steel. Positron lifetime measurement was also made clarifying if the GBE process make severe crack to deplete a performance of base metal of stainless steel.

For a solid target, tungsten is the most candidate material to give high neutron yield and to be high temperature materials. However, there are two severe problems: (1) irradiated tungsten showed fairly harden and brittle in the tensile and bending tests [10,11], although the compression test showed that tungsten had some ductility even after 23 dpa irradiation [12], (2) tungsten

* Corresponding author.
E-mail address: masayoshi.kawai@kek.jp (M. Kawai).

0022-3115/$ - see front matter © 2008 Elsevier B.V. All rights reserved.
doi:10.1016/j.jnucmat.2008.02.060

was easily corroded by flowing water with high velocity [13,14] or high temperature [15]. To the former problem, we have investigated the methods to develop the tungsten alloy which has radiation induced ductility upgrade. In this time, the radiation-resistant, ultra-fine grained tungsten materials was successfully developed.

To the latter problem, we have already established the method to fabricate the tantalum-clad tungsten target, to be used for even MW class spallation neutron sources, with hot isostatic pressing (HIP'ing) process [16,17]. However, a used tungsten target will have remarkably high radiation activities because of high neutron-activation cross sections and high-energy decay-gamma-rays of activated tantalum [18]. Such high activities bring us difficulty of exchanging the used target into the new one [19]. On the other hand, CrN has advantages for stronger corrosion resistance [15] and lower neutron-induced activity than tantalum. Accordingly, we had tried to make CrN coating on a tungsten plate with the arc-ion-plasma type PVD (AIP) technique and the ion-beam-enhanced deposition (IBED), and fundamental mechanical properties were also measured [1]. After that, a proton beam irradiation tests were made on the CrN-film on tungsten processed with the AIP technique. Electrochemical method using molten salt, that had been examined to fabricate a tantalum-clad tungsten [1,17], was also studied aiming at confirmation of production system of CrN coating in large (engineering) scale.

Investigation of pitting damage in a mercury target has been continued by using the electro-magnetic high-frequency impact generator, magnetic impact testing machine (MIMTM) [20] to input a controlled stress into various combination of materials and mercury up to some 10^8 pulses. At IWSMT-7, we showed that the surface treatment to harden stainless steel increased the impact erosion resistances but remained a problem of becoming brittle [1]. In this time, synergistic effect of nitride and carbon-diffusion for surface treatment of the 316-type stainless steel was studied. Impact test with high-speed camera observation was also made to clarify the bubble behavior at the interface between mercury and material (in the present case, glass).

2. Topics

2.1. Grain boundary engineering (GBE)

Intergranular corrosion (IGC) by a coolant water, resulting in weld decay, is frequently observed in the heat affected zone (HAZ) of austenitic stainless steel. Similar IGC may occur in a solid target. Recent studies on the grain boundary structure have revealed that the sensitization depends strongly on the crystallographic nature and the atomic structure of the grain boundary due to $Cr_{23}C_6$ precipitation, and that low-energy grain boundaries, such as CSL (coincidence site lattice) boundaries, have strong resistance to IGC [4,9], as illustrated in Fig. 1. GBE [7] is a fundamental and effective method to inhibit sensitization by increasing the frequency of CSL boundaries. There are two kinds of methods to increase low-energy grain boundary: strong work plus heat treatment leading strain recrystallization, and weak work plus heat treatment inducing strain annealing. Recently, Shimada et al. [9] demonstrated that slight pre-strain annealing at a relatively low temperature results in excellent IGC corrosion resistance due to grain boundary character distribution in type-304 austenitic stainless steel. It was found in their corrosion tests by measuring a mass-loss of specimens soaked in a ferric sulfate acid after sensitization that a corrosion rate of the GBE-controlled material with *r*5%–1200 K–72 h annealing which seemed to be optimum in a fraction of the CSL boundaries was less than one fourth that of the base metal.

In the present work, we investigated an optimum condition to obtain large CSL fractions in 316-type stainless steel by changing pre-strain rate, i.e., reduction rate between 2% and 6%. Annealing was made keeping at temperature: 1200–1300 K for 72 h. Fig. 2 shows the OIM (orientation imaging microscopy) results. Higher frequency is observed in the region of small reduction ratio between 2% and 4%. The highest frequency of 86.4% is obtained at the pre-strain of 3%, annealing temperature of 1240 K and annealing time of 72 h [21].

Positron lifetime measurement is frequently made to investigate an amount of defects in the specimen. In the present work, the measurements were performed by using a positron source of ^{22}Na for the base metal (BM) of 316-type stainless steel (SS316), its GEM-controlled material and the sample irradiated by neutron by 7.5×10^{18} n/cm^2 in JMTR. The results are given in Table 1.

Before irradiation, the positron lifetimes in the base metal of SS316 and SS316L are almost the same as those in the GEM-controlled materials. It means that the GEM process did not increase defects in material. Difference of lifetime between the SS316 and SS316L is also very small. The lifetimes in the SS316 and SS316L were larger than that in pure iron (106 ps) and pure nickel (109 ps). On the hand, even small neutron irradiation obviously

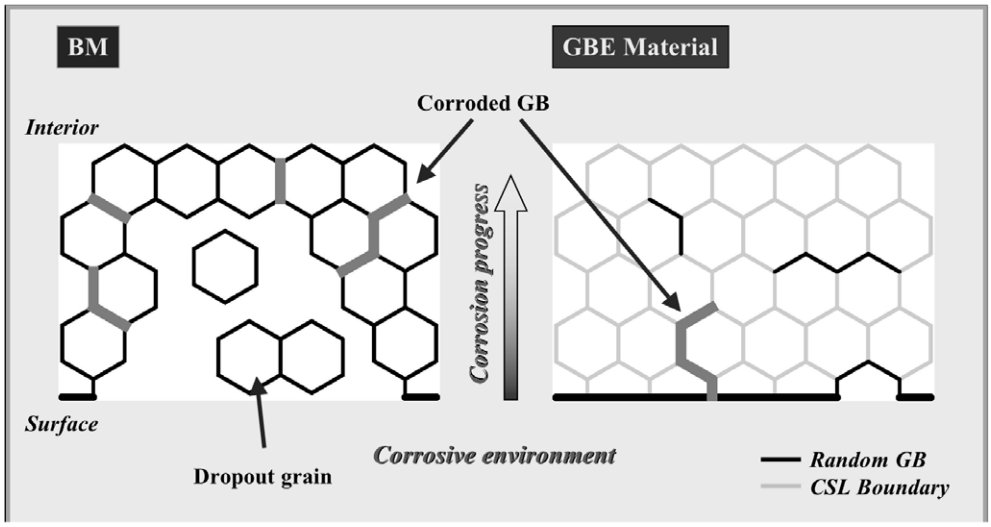

Fig. 1. Comparison of schematic corrosion process.

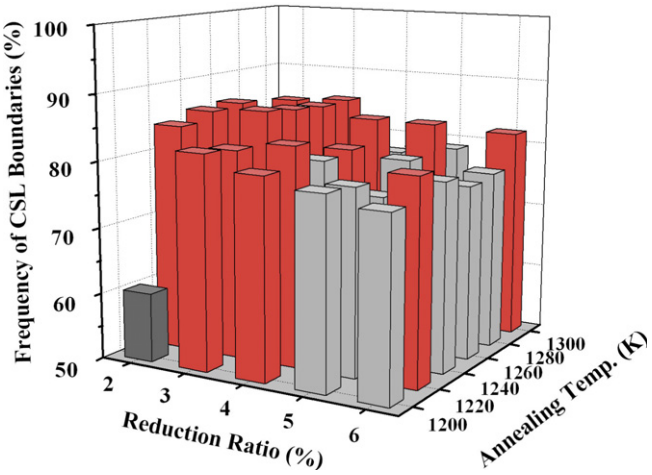

Fig. 2. CSL boundary frequency of 316 stainless steel as a function of reduction ratio and annealing temperature. Red shows CSL frequency is higher than 80%, light gray denote to between 70% and 80%, while dark gray does otherwise.

Table 1
Comparison of positron lifetimes for the stainless steel

	BM of SS316	GBEM of SS316	BM of SS316L	GBEM of SS316L
Before irradiation	121.1	121.2	119.9	122.4
Irradiated by 7.5×10^{18} n/cm^2	130.0	134.7	139.3	138.8

increased lifetime. Accordingly, the influence the GEM process can be said to be negligibly small.

2.2. Development of radiation-resistant, ultra-fine grained tungsten materials (W–TiC)

A pure tungsten that is the most useful material of a solid target has a tendency of quick increase of DBTT (ductile-brittle transition temperature) with a neutron irradiation dose. This result was obtained with the tensile and bending tests for the samples irradiated at the nuclear reactors [11]. Additionally, high energy proton beams bombarding the target of the spallation neutron source produce extremely larger amounts of gases such as proton and helium than in the nuclear reactors. Especially, helium gases enhance the radiation damage such as radiation hardening and embrittlement. Accordingly, it is required to develop a tungsten alloy resistant to irradiations with neutrons and helium ions. In the present work, ultra-fine grained W–TiC (UFG W–TiC) with a high purity matrix of low dislocation density is expected to exhibit improved resistance to irradiations with neutrons and helium ions [22]. Aiming at such UFG W–TiC with the desired microstructure, powders of W with 0.3, 0.5 and 0.8 wt% TiC additions were subjected to mechanical alloying (MA) [23] where purified H_2 and Ar were used as the MA atmosphere, followed by hot isostatic pressing (HIP). Microstructural observations by transmission electron microscopy (TEM) showed that UFG W–(0.3–0.8) wt%TiC exhibits equiaxed grains with average diameters of 50–190 nm and nearly full densification of approximately 99% (relative density). Significant grain refinement occurred by TiC additions and a high density of fine Ar bubbles were retained after HIPing of MA powders treated in a purified Ar gas [22,24]. On-line and automated analyses with orientation imaging microscopy (OIM) [25] showed that the grain boundary character distributions of W–0.5TiC–H_2 (i.e., W–0.5TiC fabricated with MA in a purified H_2 atmosphere) consist of mostly high-angle random grain boundaries with a frequency of approximately 80% [26].

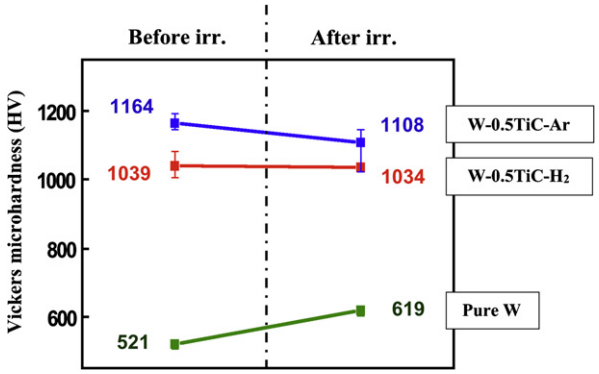

Fig. 3. Vickers microhardness before and after neutron irradiation at 873 K to 2×10^{24} n/m^2 in JMTR for pure W, W–0.5TiC–H_2 and W–0.5TiC–Ar.

Neutron irradiation test was performed for TEM disks of W–0.5TiC–H_2 and W–0.5TiC–Ar to a fluence of 2×10^{24} n/m^2 (about 0.15 dpa) at 873 K in the JMTR. For comparison, TEM disks of commercially available pure W with a grain size of approximately 20 μm in the hot-rolled, stress-relieved condition were also irradiated. Vickers microhardness test results for those specimens before and after neutron irradiation showed that W–0.5TiC–H_2 and W–0.5TiC–Ar exhibit no radiation hardening, whereas commercially available pure W with about 521 HV in unirradiated state shows a considerable hardening of ΔHV = 98, as shown in Fig. 3. In view of the previous results on fine-grained W–0.3TiC (grain size: 0.9 μm) and pure W irradiated at 563 K to 9×10^{23} n/m^2 ($E > 1$ MeV) where ΔHV was 30 for W–0.3TiC and 63 for pure W [27], we can say that the UFG microstructure in W–0.5TiC is very effective in improving the resistance to radiation hardening. In addition, 3 MeV He-ion irradiations at 823 K to 2×10^{23} He/m^2 showed that surface damage resistance for UFG W–0.3TiC–H_2 is more than ten times as high as that for the commercially available W materials [15].

These results suggest that ultra-fine grained W–TiC can possess improved performance for use under irradiation environments.

2.3. CrN film formation on tungsten

Tungsten has a weak point that it is easily corroded by flowing water with high velocity [12], especially under irradiation. In order to overcome such a weak point, cladding with corrosion resistant material was applied to tungsten target. Typical example is a tantalum-clad tungsten target for KENS [15] and ISIS [28]. However, tantalum is highly activated by thermal neutrons [18] and its decay heat is a problem during target exchange [19]. On the other hand, CrN is less activated by neutron and has higher corrosion resistance than tantalum [14]. CrN clad is frequently made with an AIP (arc ion plating) method. However, this method may be difficult for uniformly coating a large target with a sufficient thickness exceeding some tens of micrometers. Electrodeposition is extremely useful due to high flexibility for a big-size complicated shape of the objects to be coated, and has an advantage of low cost. Molten-salt electrolysis has been successfully applied for the deposition of valve metals [29] and their alloys [30].

In the present work, the authors designed the methods adding ammonium chloride as a source of nitrogen to the molten salt on the basis of the following equation:

$$x\mathrm{Me}^{z+} + y\mathrm{NH}_4^+ + (xz + y)\mathrm{e}^- \rightarrow \mathrm{Me}_x\mathrm{N}_y + 2y\mathrm{H}_2 \quad (\mathrm{Me}: \mathrm{Metal}) \qquad (1)$$

Cyclic voltammetric measurements were performed by using a Cr rod as a working electrode in a molten salt of LiCl–KCl (723 K). As shown in Fig. 4, reduction currents below 2.0 V (vs. Li^+/Li) increase with increasing additive amounts of NH_4Cl is considered to correspond to the formation of chromium nitride film

$$xCr + NH_4^+ + e^- \rightarrow Cr_xN + 2H_2 \quad (2)$$

In order to confirm the electrochemical formation of nitride films at potentials below 2.0 V according to the formation scheme (2), potentiostatic electrolysis was made by using Cr plate as a working electrode in LiCl–KCl eutectic melt containing NH_4Cl (1.0 mol%) at 0.1–1.5 V (vs. Li^+/Li) and the chromium nitride was identified on the Cr plate by X-ray analysis. Furthermore, we obtained chromium nitride layer of on tungsten after potentiostatic analysis at 1.6 V for 2 h in LiCl–KCl–CsCl–NH_4Cl (0.5 mol%)–$CrCl_2$ (0.5 mol%) eutectic melt at 573 K according to the reaction scheme (1). Chromium layer in Fig. 5 showed about 10 μm thickness that was slightly uneven, so far and was composed of CrN and Cr_2N. Future task is to search an optimum condition to make a uniform and thick CrN layer on tungsten.

Prior to the eutectic method mentioned above, we had tried to make a CrN film on tungsten plate by an arc-ion-plasma type PVD (AIP) technique and the ion-beam-enhanced deposition (IBED) [1]. With the latter method it was difficult to make a sufficiently thick film. In the present work, proton irradiation tests were made for AIP film samples prepared by the Japan Coating Center Co. Ltd., by using the 1 MeV proton beam from the Dynamitron at Tohoku University. With an assumption that the threshold energy of atomic displacement was 40 eV for CrN of 5.8 g/cm^{3}and 90 eV for tungsten, the proton range was estimated to be 7.05 μm in a sample composed of 5 μm-thick CrN film and tungsten, and 7.62 μm in the sample of the 8 μm CrN film. The purpose of each experiment was to observe blistering of tungsten by hydrogen gas accumulated in tungsten layer for thin CrN film specimen and to confirm strength to impact in case of thick CrN film specimen,

In the experiments, beam irradiation was made at the room temperature and stopped when some irradiation damage was observed: 8.3×10^{22} H^+/m^2 for 5 μm CrN and 7.3×10^{21} H^+/m^2 for 8 μm CrN. For thin sample, we observed swellings with a hundred micro-meter diameter in maximum in many places and tiny lacks.

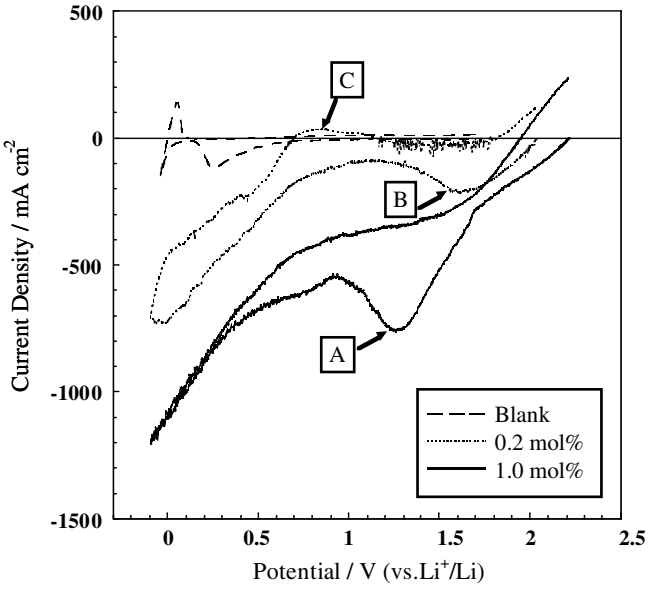

Fig. 4. Cyclic voltammograms for Cr electrode in LiCl–KCl–CsCl melt and LiCl–KCl eutectic melt adding 0.2 mol% and 1.0 mol% NH_4Cl at 573 K. Scan rate is 0.1 V/s.

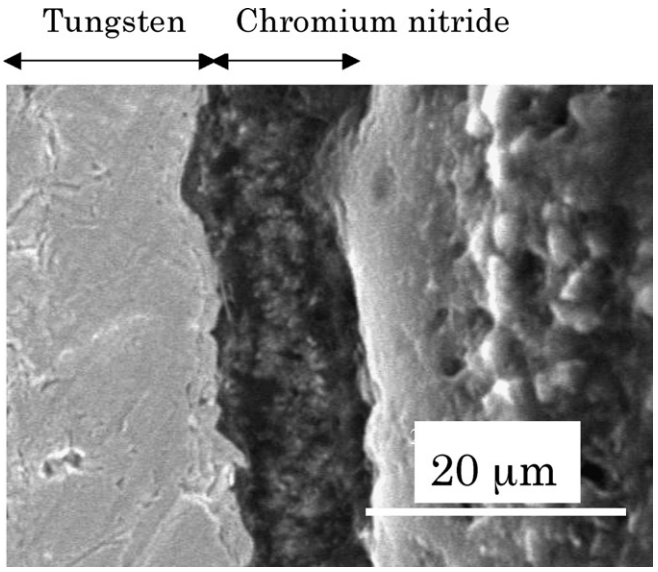

Fig. 5. Cross sectional SEM image of W sample after potentiostatic electrolysis at 1.6 V for 2 h at 573 K.

We guessed that the swelling was not a trail of the blistering which should occur in the tungsten layer, but a mere peeling-off of the CrN film from the tungsten, as tiny lacks around the swelling were considered to be an appearance of weak bonding between the CrN film and the tungsten. For thick sample, swellings and tiny lacks were observed even in lower irradiation and a crater of about 200 μm diameter was also remained: it might be caused by a droplet of vaporized-Cr ion deposition. Accordingly, it is considered that the present AIP CrN on tungsten has not a sufficient strength to beam impact.

In general, CrN film on steel materials has a excellent resistance to corrosion and wear, and it was developed for valve coating of nuclear plant [31]. However, the present experiment showed that the AIP CrN film on tungsten has weak resistance to irradiation damage. This weakness may come from some factors of the present commercial AIP method. Then, the experiments by the improved AIP method or chemical deposition would solve a problem. If there may be a problem in a compatibility between CrN and tungsten, CrN film will be difficult without a proper intermediate layer on the substrate tungsten.

2.4. Synergistic effect of C and N plasma treatment of stainless steel

Pitting damage of mercury target was investigated for various materials by using the MIMTM [20] that can give a high-frequent and strength-controlled impacts on liquid metal. Fig. 6 shows pitting damage on a low-carbon 316-type austenitic stainless steel (denoted as 'SUS316L' in the figure) and various surface treatment materials after imposing 10^6 impacts with 556 W which was corresponds to the impact produced by 1 MW proton beam with a 25 Hz repetition and 1 ms width in the spallation neutron source of the J-PARC. Surface treatments were gas nitriding, plasma nitriding, curburizing (Kolsterising@), gas nitriding plus TiN CVD (chemical vapor deposition), gas nitriding plus TiAlN CVD, plasma nitriding plus DLC (diamond like carbon) CVD and boronizing. The figure shows optical images and depth profiles taken by a laser microscope. In case of SUS316L, whole surface was damaged and depth profile showed violent undulations which were considered to come from local frequent impacts due to cavitation bubble collapse. Depth of the damage was 12 μm in maximum. Damage is very dependent on the surface treatments. Gas nitriding material

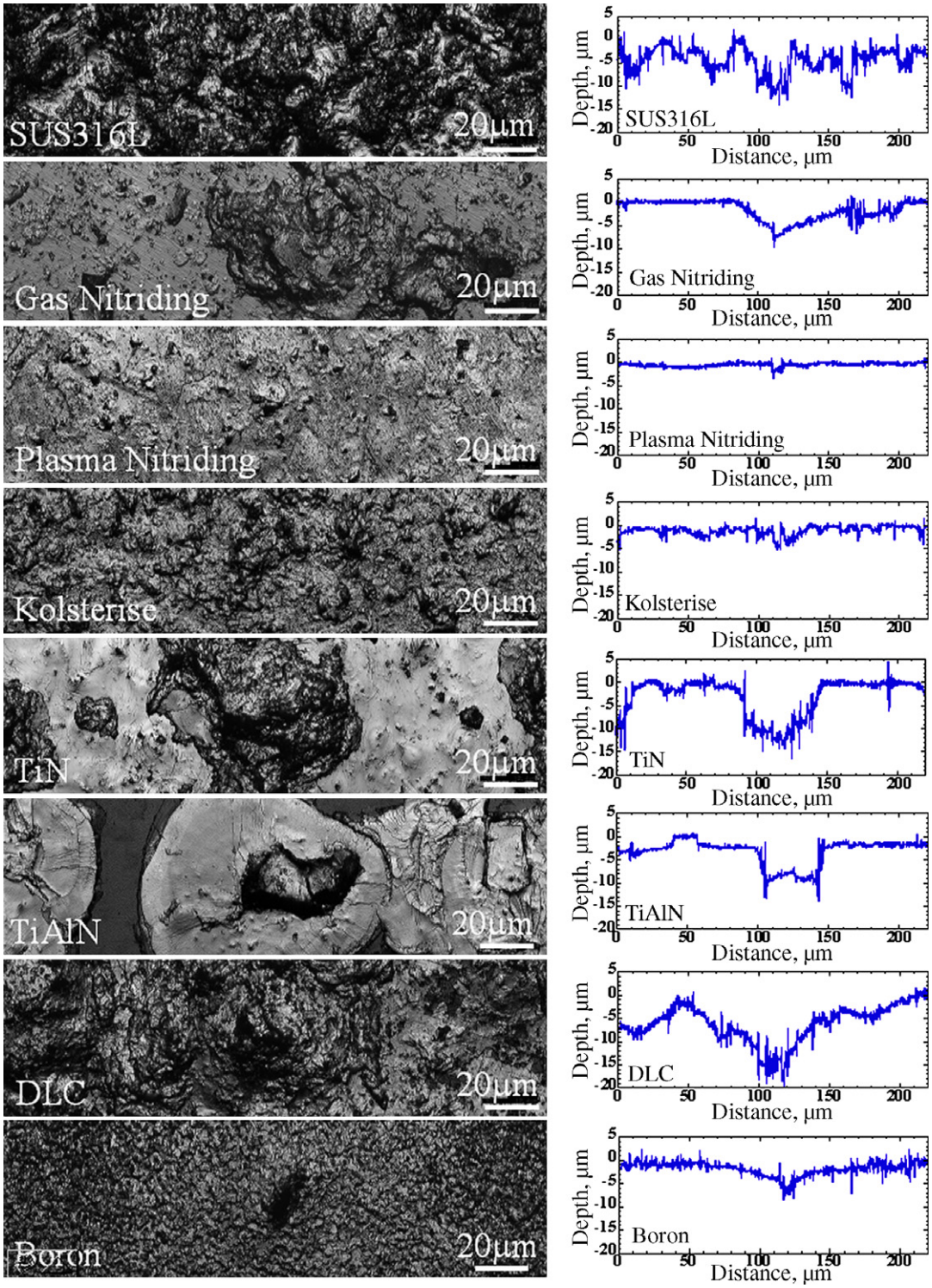

Fig. 6. Pitting damage on various surface treatments after 10^6 impacts optical images and depth profiles taken by a laser microscope.

shows large pits with about 10 μm depth. Around the pit, small cracks are observed. On the other hand, the plasma nitriding treatment exhibits the most resistant surface against the pitting damage with less and shallow pits, while the others do large or many pits.

Beyond 10^6 impacts, we obtained the data that the fatigue strength was degraded by the nitriding treatment because the whole of the improved hard surface seemed to knock the softer substrate and gave it fatigue. As a result, the nitriding treatment after 10^7 cycle impacts exhibited the severer damage than the SUS316L. A novel surface treatment taking the synergistic effect of C and N plasma treatment into account was developed to improve the surface resistance against localized impact due to cavitation bubble collapse and the fatigue strength. In the experiment, the conventional plasma nitriding was carried out at 673 K for 190 h. The plasma curburizing and nitriding were made under several combinations of temperature and time by measuring hardness distributions from the surface. Thus, it was found that the diffusion

coefficient of carbon at 673 K was 2.6 times as much as that of nitrogen and increased to 3.6 times at 723 K. Finally, we chose the condition for the complex treatment of curburizing at 723 K for 20 h and nitriding at 673 K for 190 h. Carbon diffused into about 20 μm depth in the first step of curburizing and gradually into 50 μm in the second step. This carbon density change gives a gradually changing hardness. The impact tests by using the MIMTM were made for SS316, conventional nitriding SS316 and the material with the complex treatment of curburizing and nitriding.

Fig. 7 shows 3D image of the pitting-damaged specimens up to 10^7 impacts with 556 W, observed by a laser microscope. Undamaged surfaces were not observed in SUS316L and nitriding one. In particular, nitriding specimen shows deep hollow because of fatigue failure as mentioned above.

2.5. Bubble behavior observation

In order to decrease influence of the pitting damage, it is important to investigate bubble behavior near the interface between mercury and window/vessel material and to develop the methods to simulate the phenomena and estimate pitting damage with a good accuracy. Visualization of cavitation bubble formation was made by using a high-speed video camera (Hyper Vision HPV-1, Shimadzu) whose frame rate was 10^6 f/s. The bubble was formed on the interface between mercury and a glass window, which was installed in a lid of the mercury chamber. A trigger signal was precisely controlled and input from the MIMTM to the camera at the onset of the electro-magnetic striker driving to investigate the relationship between time response of imposed pressure in mercury and acceleration measured at the striker and the optical images of bubbles.

Fig. 8 shows the typical pictures taken by the high-speed video camera, which caught the bubble collapse behavior with micro-jet impact. The micro-jet collided vertically against the glass window and spread out on the surface of glass window. The speed of mercury spreading V_s was estimated to be 200–300 m/s from the pictures. This velocity is corresponding to the impact velocity to make the pitting.

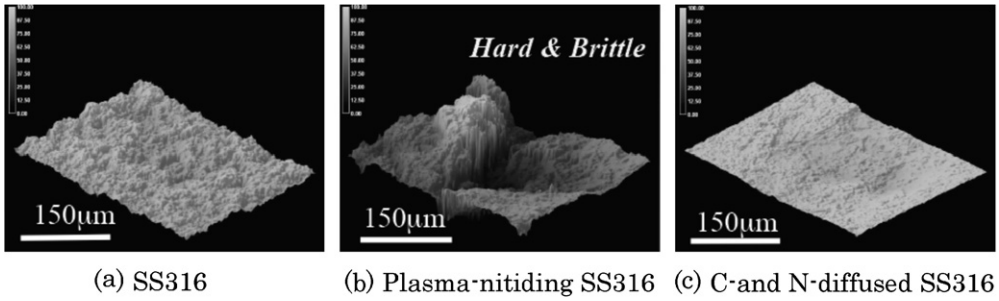

Fig. 7. Comparison of surface figure observed by laser-microscope for pitting-damaged specimens of SS316, plasma-nitriding SS316 and C- and N-diffused SS316 after 10^7 cycle impacts of 560 W given by the MIMTM.

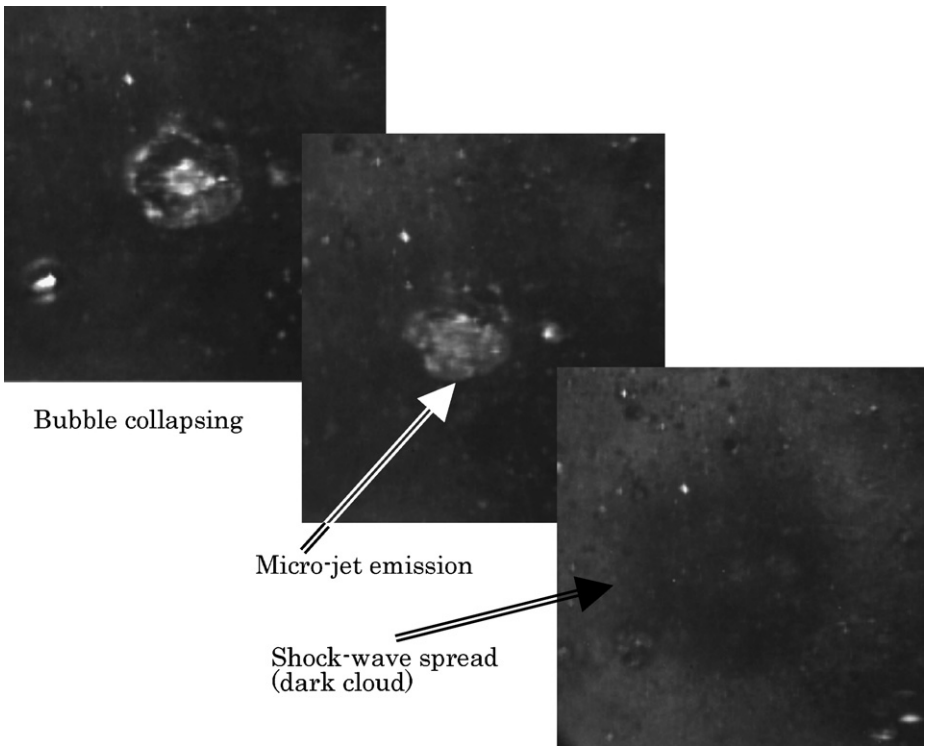

Fig. 8. Observation of bubble behavior near mercury and glass interface.

3. Summary

The present work has been performed to develop materials which have strong resistance to both beam impact and radiation damage. Such materials are required for the beam target of an intense accelerator. In the present paper, the authors introduced the works on the spallation materials. Main results are as follows:

(1) The GBE controlled SS316, which is a candidate material of vessel and the window of the spallation target, has advantage of inter-granular corrosion (IGC) resistance on coolant water and possibility of high resistance to radiation damage. Weak pre-strain of only 3% was the best condition to increase the coincidence site lattice boundaries giving a property of IGC resistance. Any influence of the GBE process to producing material defects did not observed by the positron lifetime measurement, while it exhibited irradiation effects even small neutron dose of 7.5×10^{18} n/cm^2 in the JMTR.
(2) Pure tungsten that has disadvantages of becoming brittle under irradiation circumstances and being corroded by a flowing water. Radiation-resistant, ultra-fine grained tungsten materials dispersed with TiC fine powder (W–TiC) was successfully developed instead of the pure tungsten. Neutron irradiation test of W–TiC showed that it kept the ductility or became softer. It will be hopeful as a solid target material. To guard from the corrosion by water, a CrN film is ideal because of higher corrosion resistance and lower activation than tantalum. Molten salt technique has been attained to be several micro-meter thickness of the CrN film on the tungsten layer. Since the uniformity of layer thickness is not sufficient, further investigation will be needed to make a uniform and strong bonding film. On the other hand, it has been observed that the AIP CrN film on tungsten was not sufficiently strong to beam impact, so far.
(3) For liquid mercury target, pitting damage of the vessel and window is a sever problem. In the MIMTM experiments, surface treatment of SAS316 stainless steel seemed to be effective below 10^6 impacts but lost its effects against more impacts. In order to reduce the pitting damage, C and N plasma surface treatment has been developed and proven to be effective to suppress pitting damage under such a large amount of impacts. This technique will give us a clue of more tough materials against the pitting damage.
(4) Another method to reduce the pitting damage is to suppress the stress of the pressure waves due to mercury bubble collapsing. High-speed camera clarified bubble behavior near mercury/glass window surface. The results will give the fundamental data to evaluate the effects of pressure waves through the computer simulation and this experiments will be effective to find the mitigation technique of the impacts due to proton beam.

Acknowledgements

This work has been performed under the support by 2004–2006 FY Grant-in-Aid for Science Research (A) by JSPS, Task No. 16206097 'Creation of Intelligent Materials with a Resistance to Beam-Impact and Radiation Damage'.

References

[1] M. Kawai, H. Kokawa, H. Okamura, A. Kawasaki, T. Yamamura, N. Hara, N. Akao, M. Futakawa, K. Kikuchi, J. Nucl. Mater. 356 (2006) 16.
[2] E. Folkhard, Welding Metallurgy of Stainless Steels, Springer-Verlag, Vienna, 1988. p. 103.
[3] H. Kokawa, M. Shimada, M. Michiuchi, Z.J. Wang, Y.S. Sato, Acta Mater. 55 (2007) 5401.
[4] H. Kokawa, M. Shimada, Y.S. Sato, JOM 52 (2000) 34.
[5] H.Y. Bi, H. Kokawa, Z.J. Wang, M. Shimada, Y.S. Sato, Scripta Mater. 49 (2003) 219.
[6] T. Watanabe, Res. Mech. 11 (1984) 47.
[7] G. Palumbo, E.M. Lehockey, P. Lin, JOM 50 (1998) 40.
[8] H. Kokawa, J. Mater. Sci. 40 (2005) 927.
[9] M. Shimada, H. Kokawa, Z.J. Wang, Y.S. Sato, I. Karibe, Acta Mater. 50 (2002) 2331.
[10] H. Ulmaier, F. Carsughi, Nucl. Instrum. and Meth. B 101 (1995) 406.
[11] J.W. Davis, V.R. Barabash, A. Makhankov, L. Ploechl, K.T. Slattery, J. Nucl. Mater. 258–263 (1998) 308.
[12] S.A. Maloy, M.R. James, W. Sommer Jr., G.J. Wilcutt Jr., M. Lopetz, T.J. Romero, M.B. Toloczko, J. Nucl. Mater. 343 (2005) 219.
[13] N. Noji, K. Kashiwagura, N. Akao, S. Soma, N. Hara, K. Sugimoto, J. Jpn. Inst. Met. 66 (2002) 1107 (in Japanese).
[14] M. Kawai, M. Furusaka, K. Kikuchi, H. Kurishita, R. Watanabe, J.-F. Li, K. Sugimoto, T. Yamamura, Y. Hiraoka, K. Abe, A. Hasegawa, M. Yoshiie, N. Takenaka, K. Mishima, Y. Kiyanagi, T. Tanabe, N. Yoshida, T. Igarashi, J. Nucl. Mater. 318 (2003) 38.
[15] Y. Ishijima, K. Kakiuchi, T. Furuya, H. Kurishita, M. Hasegawa, T. Igarashi, M. Kawai, J. Nucl. Mater. 307–311 (2002) 1369.
[16] M. Kawai, K. Kikuchi, H. Kurishita, J. Li, M. Furusaka, J. Nucl. Mater. 296 (2001) 312.
[17] M. Kawai, M. Furusaka, J.-F. Li, A. Kawasaki, T. Yamamura, M. Mehmood, H. Kurishita, K. Kikuchi, N. Takenaka, Y. Kiyanagi, T. Igarashi, M. Katoh, Solid Spallation Target Materials Development, in: Proceedings of the ICANS-XVI, ESS 03-136-M1, vol. II, 2003, p. 1087.
[18] D. Nio, M. Ooi, N. Takenaka, M. Furusaka, M. Kawai, K. Mishima, Y. Kiyanagi, J. Nucl. Mater. 343 (2005) 163.
[19] N. Takenaka, D. Nio, Y. Kiyanagi, K. Mishima, M. Kawai, M. Furusaka, J. Nucl. Mater. 343 (2005) 169.
[20] M. Futakawa, T. Naoe, H. Kogawa, C. Tsai, Y. Ikeda, J. Nucl. Sci. Technol. 40 (2003) 895.
[21] M. Michiuchi, H. Kokawa, Z.J. Wang, Y.S. Sato, K. Sakai, Acta Mater. 54 (2006) 5179.
[22] H. Kurishita, S. Kobayashi, K. Nakai, H. Arakawa, S. Matsuo, T. Takida, K. Takebe, M. Kawai, Phys. Scripta T128 (2007) 76.
[23] J.S. Benjamin, Metall. Trans. 5 (1970) 2943.
[24] H. Kurishita, S. Kobayashi, K. Nakai, T. Ogawa, A. Hasegawa, K. Abe, H. Arakawa, S. Matuso, Y. Hiraoka, T. Takida, K. Takebe, M. Kawai, N. Yoshida, J. Nucl. Mater. 377 (2008) 34.
[25] B.L. Adams, Metall. Trans. A 24 (1993) 819.
[26] H. Kurishita, S. Tsurekawa, T. Matsuzaki, S. Kobayashi, K. Nakai, H. Arakawa, T. Takida, K. Takebe, Mater. Sci. Eng. A, submitted for publication.
[27] H. Kurishita, Y. Amano, S. Kobayashi, K. Nakai, H. Arakawa, Y. Hiraoka, T. Takida, K. Takebe, J. Nucl. Mater. 367–370 (2007) 1453.
[28] A.D. Taylor, The ISIS Second Target Station, in: Proceedings of the ICANS-XVI, the 16th Meeting of the International Collaboration on Advanced Neutron Sources, May 12–15, 2003, Deusseldorf-Neuss, Germany, vol. I, 2003, p. 73, ISSN 1433-559X.
[29] S. Senderoff, G.W. Mellors, W.J. Reinhart, . J. Electrochem. Soc. 8 (1965) 266.
[30] M. Mehmood, N. Kawaguchi, Y. Sato, T. Yamamura, J. Alloys Compd. 287 (1999) 91.
[31] N. Kitagawa, PVD Ceramic Coatings For Valve Seats, in: Proceedings of 3rd Workshop on the Materials Science and Technology for Spallation Neutron Source, KEK Proceedings 2002–6, 2002, p. 103.